

## Plasma ionization balance in chemical-picture and average-atom models

A. A. Ovechkin <sup>1,\*</sup>, P. A. Loboda <sup>1,2</sup>, V. V. Popova,<sup>1</sup> E. Yu. Akulinina <sup>1</sup>, M. E. Berezovskaya,<sup>1</sup>  
A. S. Korolev,<sup>1</sup> and S. V. Kolchugin<sup>1</sup>

<sup>1</sup>*Russian Federal Nuclear Center—Zababakhin All-Russian Research Institute of Technical Physics (RFNC-VNIITF),  
13, Vasilyeva st., Snezhinsk, Chelyabinsk region 456770, Russia*

<sup>2</sup>*National Research Nuclear University—Moscow Engineering Physics Institute (MEPhI), 31, Kashirskoe sh., Moscow 115409, Russia*



(Received 21 December 2022; accepted 2 July 2023; published 31 July 2023)

We propose an approximate method to calculate ion partition functions in the context of the chemical-picture representation of plasmas as an interacting mixture of various ions and free electrons under the local-thermodynamic-equilibrium conditions. The method uses the superconfiguration approach and implies that the first-order corrections to the energies of excited electron configurations due to the electron-electron interaction may be replaced by a similar first-order correction to the energy of the basic configuration of an ion with the same number of bound electrons. The method enables one to significantly speed up the calculations and generally provides quite accurate results. Using the method proposed, plasma ionization balance and average ion charges calculated on the base of the chemical-picture representation show a good agreement with the relevant average-atom data. For the case of weak electron-ion nonideality, we provide approximate relations between the chemical-picture and average-atom values of the average ion charge, chemical potential, and plasma-density depression of ionization potential.

DOI: [10.1103/PhysRevE.108.015207](https://doi.org/10.1103/PhysRevE.108.015207)

### I. INTRODUCTION

Thermophysical properties of high-temperature plasmas in a wide range of temperatures and densities are most frequently described with quantum-statistical models of two types: ionization equilibrium or chemical-picture models [1–9], that represent the matter as an interacting mixture of various ions with the internal electronic (atomic-shell) structure and free electrons and average-atom models [10–12] based on the electron-density functional theory [13,14] and dealing with microscopic quantities averaged over all possible quantum ion states. With a few exceptions (see, e.g., Refs. [5,7,9,15–18]), chemical-picture models are generally used for low-density plasmas (at densities smaller or much smaller than that of the normal solid), while the average-atom models, on the contrary, are used for the compressed matter. However, the applicability domains of these models largely overlap with each other if the density and atomic-shell-structure effects are appropriately taken into account. In this context, it is important to perform a comparative analysis of chemical-picture and average-atom models as it enables one to provide mutual verification and a deeper understanding of underlying approximations of the models, and it makes the simulation of thermophysical plasma properties more reliable. In particular, it is essential to compare the relevant ionization-balance and average-ion-charge calculated data since these data directly affect the modeled thermodynamic and optical properties. Also, calculated data on average ion charges are necessary to address a number of special issues such as the

evaluation of electron (electric and thermal conductivities, thermoelectric power) [19–23] and ion (viscosity and diffusion) [24,25] transport coefficients and Thomson scattering cross-sections [26–28], energy loss of fast charged particles in various materials [29], and construction of ion-ion pair potentials for molecular-dynamics simulations using, e.g., the method of pseudoatom molecular dynamics [30,31]. In this context, we note that available experimental data on average ionization of dense high-temperature plasmas are rather scarce (see, e.g., Refs. [32–34]). It is also worth noting that average ion charge is a nonobservable quantity that may be defined for the average-atom model in several ways. These definitions and the effect of their use on the calculated quantities were studied in detail in previous papers [19,31,35–42]. By contrast, chemical-picture models give only one definition for the average ion charge. At the same time, only a few papers can be found where chemical-picture and average-atom models are subject to comparative analysis [43], including the comparison of average ion charges that the models give [44–46]. The present work provides such a comparison regarding a version of the chemical-picture model we previously developed and called CP-SC (chemical-picture superconfiguration model) [6], and one of the most commonly used average-atom models—the Liberman model [47].

The CP-SC model calculates ion partition functions using the superconfiguration (SC) approach [48,49] and the occupation-probability formalism for one-electron states in the presence of plasma electric microfields [3]. The model includes the effects of Coulomb nonideality and electron degeneracy, thus allowing its use in a wide range of temperatures and densities up to the values at which pressure ionization becomes essential. We will not discuss all the features of the

\*ovechkin.an@mail.ru

CP-SC model here, and we address the issues instead that were not detailed in Ref. [6] and had yet to be pursued, namely calculation of the ionization balance and the account of the first-order correction to the configuration energy due to the electron-electron interaction.

At present, Liberman's model has been implemented in a number of average-atom codes [50–53]. We use our own implementation—the RESEOS model [54,55]. A method to calculate ionization balance with RESEOS is described in Ref. [54], and we will not go into the details here.

In Sec. II we describe a method employed in the CP-SC model to calculate ion partition functions using the SC approach allowing for the first-order correction to the configuration energy due to electron-electron interaction, and we compare charge-state distributions of iron plasmas obtained from the CP-SC and RESEOS calculations. Section III is devoted to comparisons of average ion charges calculated with various models.

## II. IONIZATION BALANCE IN THE SUPERCONFIGURATION APPROXIMATION

In the CP-SC model, the ionization balance is found by solving the modified Saha equations [56] (see, e.g., Ref. [4]):

$$\frac{c_Q}{c_{Q-1}} = \frac{U_Q(\mathbf{g})}{U_{Q-1}(\mathbf{g})} \exp[\beta(\mu_e - \Delta\tilde{\mu}_Q)], \quad (1)$$

$$Z - \sum_Q c_Q Q = \langle Z \rangle = \frac{\sqrt{2}}{\pi^2 \beta^{3/2} n_i} I_{1/2}(\beta \mu_e), \quad (2)$$

$$\sum_Q c_Q = 1. \quad (3)$$

Here  $Z$  is the nuclear charge,  $\langle Z \rangle$  is the average ion charge,  $c_Q$  is the fractional abundance of ions with  $Q$  bound electrons,  $\beta = 1/T$  ( $T$  stands for the temperature),  $\mu_e$  is the electron chemical potential,  $n_i$  is the ion density,  $I_k(x) = \int_0^\infty \frac{y^k dy}{1 + \exp(y-x)}$  is the Fermi-Dirac integral, and  $\Delta\tilde{\mu}_Q$  denotes the nonideality correction given by the difference of the chemical-potential corrections of particles involved in the ionization-recombination process:

$$\Delta\tilde{\mu}_Q = \left( \frac{\partial}{\partial c_Q} - \frac{\partial}{\partial c_{Q-1}} - \frac{\partial}{\partial \langle Z \rangle} \right) F_C - T \sum_{Q'} c_{Q'} \left( \frac{\partial}{\partial c_Q} - \frac{\partial}{\partial c_{Q-1}} - \frac{\partial}{\partial \langle Z \rangle} \right) \ln U_{Q'} \quad (4)$$

with  $F_C$  being the per-atom energy of Coulomb interaction between ions and free electrons.

The symbol  $\mathbf{g}$  in Eq. (1) stands for the set of statistical weights  $g_s = 2j_s + 1$  of (relativistic) electron shells, with  $j_s$  denoting the total angular momentum of a shell  $s$ . The main feature of the CP-SC model is that the ion partition functions

$$U_Q(\mathbf{g}) = \sum_{C \in Q} w_C e^{-\beta E_C} \prod_s w_s^{q_s} \quad (5)$$

are calculated in the SC approximation [48,49] allowing for contributions from essentially all the excited ion states without resorting to the explicit accounting of those that frequently becomes almost intractable. Summation in Eq. (5) is performed

over all the electron configurations of a  $Q$ -electron ion with their average energies  $E_C$  and degeneracies

$$w_C = \prod_s \binom{g_s}{q_s} = \prod_s \frac{g_s!}{q_s! (g_s - q_s)!}, \quad (6)$$

with  $q_s$  being the occupation number of a shell  $s$ . In Eq. (5),  $w_s = w_s^{(Q)}(\rho, T)$  [3] ( $\rho$  stands for the material density) is the occupation probability of shell  $s$  one-electron states under the effect of a plasma ion microfield. In dense plasmas, ion-microfield perturbations lead to delocalization of the upper-shell electrons, thus truncating the number of bound-electron states and providing convergence of a  $Q$ -electron ion partition function.

The average configuration energy entering Eq. (5) is expressed as (see, e.g., Refs. [57,58])

$$E_C = \sum_s q_s \langle s \rangle + \frac{1}{2} \sum_{st} q_s (q_t - \delta_{st}) \langle s, t \rangle, \quad (7)$$

where  $\delta_{st}$  is the Kronecker delta,  $\langle s \rangle$  is the energy of a shell  $s$  electron in the Coulomb field of the nucleus (the sum of kinetic and potential energies), and  $\langle s, t \rangle$  is the interaction matrix element for electrons in shells  $s$  and  $t$ .

It should be noted that CP-SC, like most of the chemical-picture models, employs the precalculated isolated-ion data on matrix elements  $\langle s \rangle$ ,  $\langle s, t \rangle$ . In the present paper, we do not consider the class of models [5,9,15–18,44,59,60] which imply the solution of the self-consistent-field equations for electron wave functions in various ion species at each specific value of temperature and density. Such models can also be considered as the chemical-picture ones, though they do not necessarily imply the need for the solution of the Saha equations. Hence, all our further conclusions are restricted to the chemical-picture models like CP-SC in which the atomic data, expressed solely in terms of electron wave functions, are obtained for isolated ions. The important feature of the latter models is the use of the approximation of the uniform free-electron density in Eq. (2).

In the CP-SC model, the energy expressed by Eq. (7) is found from the perturbation theory: one-electron wave functions and the corresponding matrix elements  $\langle s \rangle$ ,  $\langle s, t \rangle$  are calculated for basic configurations of  $Q$ -electron ion species by using the flexible atomic code (FAC) [61] and then employed to calculate the energies of all the excited configurations of relevant ion species. The basic configurations are obtained by successively filling the electron shells in the increasing order of the principal quantum number, then of the orbital quantum number, and finally of the total angular momentum.

The main advantage of the SC approach comes from the possibility to calculate partition functions (5) by using recursion relations [48,49], thus avoiding the need for explicit accounting of individual electron configurations. The CP-SC model implements the recursion relation of Ref. [49] that offers a pathway for robust calculations at arbitrary temperatures and shell numbers. However, Eq. (7) is still inappropriate for direct use in the recursion relation since the latter suggests that the configuration energy is represented as a sum of independent contributions of individual electron shells involved. For this reason, the following approximation is generally

employed [8,62]. The configuration energy (7) is decomposed into two terms: a zero-order term  $E_C^{(0)}$ , defined as a linear expansion in terms of the electron-shell occupation numbers,

$$E_C^{(0)} = \sum_s \theta_s q_s, \quad (8)$$

and a first-order electron-electron interaction correction  $E_C^{(1)}$  that enters the calculation of the partition function of a  $Q$ -electron ion  $U_Q(\mathbf{g})$  (5) in an averaged form  $\langle E_C^{(1)} \rangle$  with the averaging done by using zero-order configuration energies. To reduce the inaccuracies due to the use of  $\langle E_C^{(1)} \rangle$  in the calculation of  $U_Q(\mathbf{g})$ , the averaging involves the sets of configurations with close average energies—superconfigurations (SCs)  $\Xi$ —rather than all the number of electron configurations of a  $Q$ -electron ion under consideration. As a result, the ion partition function is found as a sum of partition functions of individual SCs:

$$U_Q(\mathbf{g}) = \sum_{\Xi \in Q} \exp(-\beta \langle E_C^{(1)} \rangle_{\Xi}) U_{\Xi}^{(0)}(\mathbf{g}). \quad (9)$$

Here, we introduced the notation

$$U_{\Xi}^{(0)}(\mathbf{g}) = \sum_{C \in \Xi} w_C e^{-\beta E_C^{(0)}} \prod_s w_s^{q_s} \quad (10)$$

and

$$\langle A(\mathbf{q}) \rangle_{\Xi} = \frac{1}{U_{\Xi}^{(0)}(\mathbf{g})} \sum_{C \in \Xi} A(\mathbf{q}) w_C e^{-\beta E_C^{(0)}} \prod_s w_s^{q_s}, \quad (11)$$

where  $A(\mathbf{q})$  is an arbitrary function of the shell occupation numbers.

In practice, to calculate zero-order partition functions (10) with the recursion relation, SCs are represented as the collections of supershells  $\sigma$ —groups of shells with close one-electron energies—occupied by  $Q_{\sigma}$  electrons [48]. So, each SC includes all possible configurations relevant to a specified set  $\{Q_{\sigma}\}$  of the supershell total occupation numbers

$$Q_{\sigma} = \sum_{s \in \sigma} q_s. \quad (12)$$

Inaccuracies due to the use of an averaged form of the first-order electron-electron interaction correction  $\langle E_C^{(1)} \rangle_{\Xi}$  rather than the set of corrections  $E_C^{(1)}$  for individual configurations depend both on the number of supershells comprising the total set of electron shells (the more detailed the partitioning is, the better is the resulting accuracy) and on the choice of the expansion coefficients  $\theta_s$  in Eq. (8), generally being specific for individual SCs. In this context, one should note an approach developed in Refs. [63,64] based on the Gibbs-Bogoliubov (or Jensen-Feynman) inequality that provides a possibility to minimize the inaccuracies discussed with an optimal choice of the coefficients  $\theta_s$ .

If the ionization balance is calculated with an average-atom model [in this case the factor  $\prod_s w_s^{q_s}$  is missing from Eq. (10)], the matrix elements  $\langle s \rangle$ ,  $\langle s, t \rangle$  are assumed to be identical for all ion species as those are obtained under the average-atom approximation. Moreover, minimizing the inaccuracy of the total partition function  $U(\mathbf{g}) = \sum_Q U_Q(\mathbf{g})$ , one can also get the factors  $\theta_s$  to be the same for all ion species. In this case, the

values of  $\theta_s$  were found to be close to one-electron energies in the average-atom approximation:  $\theta_s \approx \varepsilon_s^{\text{AA}}$  [63,64]. Making use of this fact, we therefore take in RESEOS the zero-order approximation for the configuration energy in the form

$$E_C^{(0)} = \sum_s \varepsilon_s^{\text{AA}} q_s. \quad (13)$$

Then, if the first-order correction  $E_C^{(1)}$  is completely neglected, the well-known binomial distribution for the configuration probabilities  $P_C$  is recovered:

$$P_C = \prod_s \binom{g_s}{q_s} [n(\varepsilon_s^{\text{AA}})]^{q_s} [1 - n(\varepsilon_s^{\text{AA}})]^{g_s - q_s}, \quad (14)$$

where  $n(\varepsilon)$  is the Fermi-Dirac distribution:

$$n(\varepsilon) = \frac{1}{1 + \exp[\beta(\varepsilon - \mu_e^{\text{AA}})]}. \quad (15)$$

In Eq. (15), the electron chemical potential obtained in the average-atom approximation is denoted as  $\mu_e^{\text{AA}}$  to be distinguished from the chemical potential  $\mu_e$  entering Eqs. (1) and (2).

Although the binomial distribution overestimates the variance of the charge-state distribution [65], it enables one to reproduce exactly the average number of bound electrons obtained with the average-atom model due to the optimal choice of the expansion coefficients  $\varepsilon_s^{\text{AA}}$  in Eq. (13).

As in the average-atom model, CP-SC also treats one-electron shell energies as the coefficients of zero-order configuration energy expansion in terms of the electron-shell occupation numbers, like in Eq. (13), except that all  $Q$ -electron ion species employ their individual sets of one-electron energies:

$$E_C^{(0)} = \sum_s \varepsilon_s^{(Q)} q_s. \quad (16)$$

The energy  $\varepsilon_s^{(Q)}$  is calculated for the basic configuration of a  $Q$ -electron ion if the occupation number  $q_s^{(Q)}$  of a shell  $s$  in it is nonzero and for the relevant singly excited configuration if not. The singly excited configuration is obtained by promoting one electron from an outer (partially) filled shell of the basic configuration to the shell  $s$ . Let  $q_t^{(Q,s)}$  be the occupation number of a shell  $t$  in a configuration (basic or singly excited) for which the energy  $\varepsilon_s^{(Q)}$  is calculated. Then this energy is written as [57,58]

$$\varepsilon_s^{(Q)} = \langle s \rangle + \sum_t (q_t^{(Q,s)} - \delta_{st}) \langle s, t \rangle. \quad (17)$$

The energy expressed by Eq. (16) is, however, not so optimal as to minimize inaccuracies of the calculated partition functions. As will be shown below, for this reason calculations in the zero-order approximation (with the first-order electron-electron interaction corrections omitted) by the CP-SC model may yield rather poor estimates of the average numbers of bound electrons.

In the superconfiguration chemical-picture models, one-electron energies—the coefficients of zero-order configuration energy expansion (16)—are generally found for every individual superconfiguration by solving appropriate self-consistent-field (SCF) equations [8], which are, however,

rather expensive computationally. The CP-SC model utilizes a more efficient approach, in which the SCF equations are solved only once for the basic configurations of individual  $Q$ -electron ion species so that the energies and wave functions of electrons missing in the basic configurations are found by solving the relevant one-electron Dirac equations with the “frozen” core-electron wave functions. In this case, the amount of atomic data required for the follow-on ionization-balance calculation (matrix elements  $\langle s \rangle = \langle s \rangle^{(Q)}$ ,  $\langle s, t \rangle = \langle s, t \rangle^{(Q)}$ , and one-electron energies  $\varepsilon_s^{(Q)}$ ) is not large. Doing so, we show below that the CP-SC model yields quite accurate results if the first-order electron-electron interaction correction  $E_C^{(1)}$  to the configuration energy is taken into account.

It follows from Eqs. (7), (16), and (17) that in the CP-SC model, the first-order correction  $E_C^{(1)}$  has the form

$$E_C^{(1)} = \sum_{st} q_s \left( \frac{1}{2} (q_t - \delta_{st}) - (q_t^{(Q,s)} - \delta_{st}) \right) \langle s, t \rangle, \quad (18)$$

and its average value is

$$\begin{aligned} \langle E_C^{(1)} \rangle_{\Xi} = & \sum_{\sigma=1}^{N_{\sigma}} \left\{ A^{(Q)}(\sigma, Q_{\sigma}) \right. \\ & \left. + \sum_{s \in \sigma} \langle q_s \rangle_{\sigma} \left( \sum_{\sigma'=\sigma+1}^{N_{\sigma}} B^{(Q)}(\sigma', Q_{\sigma'}, s) - C^{(Q)}(s) \right) \right\}, \quad (19) \end{aligned}$$

where  $N_{\sigma}$  is the number of supershells,

$$A^{(Q)}(\sigma, Q_{\sigma}) = \frac{1}{2} \sum_{s,t \in \sigma} \langle q_s (q_t - \delta_{st}) \rangle_{\sigma} \langle s, t \rangle, \quad (20)$$

$$B^{(Q)}(\sigma, Q_{\sigma}, s) = \sum_{t \in \sigma} \langle q_t \rangle_{\sigma} \langle s, t \rangle, \quad (21)$$

$$C^{(Q)}(s) = \sum_t (q_t^{(Q,s)} - \delta_{st}) \langle s, t \rangle. \quad (22)$$

Average values entering Eqs. (19)–(21) are expressed in terms of the ratios of the supershell partition functions. To evaluate those, it is convenient to count off one-electron energies from their minimal values regarding each supershell:

$$\langle q_s \rangle_{\sigma} = \frac{g_s X_s \bar{U}_{Q_{\sigma}}^{(0)}(\mathbf{g}^s)}{\bar{U}_{Q_{\sigma}}^{(0)}(\mathbf{g})}, \quad (23)$$

$$\langle q_s (q_t - \delta_{st}) \rangle_{\sigma} = \frac{g_s g_t^s X_s X_t \bar{U}_{Q_{\sigma}}^{(0)}(\mathbf{g}^{st})}{\bar{U}_{Q_{\sigma}}^{(0)}(\mathbf{g})}. \quad (24)$$

Here,

$$(\mathbf{g}^{st\dots})_m = g_m^{st\dots} = g_m - \delta_{sm} - \delta_{tm} - \dots \quad (25)$$

is the reduced statistical weight of a shell  $m$ ,

$$X_s = \exp \left[ -\beta (\tilde{\varepsilon}_s^{(Q)} - \tilde{\varepsilon}_{\min}^{\sigma}) \right], \quad (26)$$

$$\tilde{\varepsilon}_s^{(Q)} = \varepsilon_s^{(Q)} - \frac{1}{\beta} \ln w_s^{(Q)}, \quad (27)$$

$$\tilde{\varepsilon}_{\min}^{\sigma} = \min_{s \in \sigma} \tilde{\varepsilon}_s^{(Q)}, \quad (28)$$

$$\bar{U}_{Q_{\sigma}}^{(0)}(\mathbf{g}) = \sum_{q_s=Q_{\sigma}} \prod_{s \in \sigma} \binom{g_s}{q_s} X_s^{q_s}. \quad (29)$$

The replacement of one-electron energies  $\varepsilon_s^{(Q)}$  by their effective counterparts (27), performed to write down Eq. (26), is done to reproduce the multiplier  $\prod w_s^{q_s}$  entering Eq. (10).

Prior to the summation over SCs in Eq. (9), it is necessary first to calculate partition functions (29) for the occupation numbers of the supershells  $Q_{\sigma}^{\min} \leq Q_{\sigma} \leq Q_{\sigma}^{\max}$  which may be encountered with a substantial probability at a given temperature and density. The set of supershells is usually constructed so that the differences of one-electron energies in each supershell are less than or of the order of the temperature value specified (to ensure the convergence with respect to the number of supershells), thus making all the factors (26) be of the order of unity. In this situation, one can use a simplified version of the double recursion relation of Ref. [49]:

$$\begin{aligned} \bar{U}_{Q_{\sigma}}^{(0)}(\mathbf{g}) & \equiv \bar{U}_{Q_{\sigma}, N}^{(0)}(\mathbf{g}) = \sum_{q=0}^{\min(Q_{\sigma}, g_N)} \bar{U}_{Q_{\sigma}-q, N-1}^{(0)}(\mathbf{g}) \\ & \times \exp \left[ -\beta (\tilde{\varepsilon}_N^{(Q)} - \tilde{\varepsilon}_{\min}^{\sigma}) + \ln \binom{g_N}{q} \right], \\ \bar{U}_{Q_{\sigma}, 0}^{(0)}(\mathbf{g}) & = \delta_{Q_{\sigma}, 0}, \quad (30) \end{aligned}$$

where  $N$  is the number of shells in a supershell  $\sigma$ . Equation (30) provides a capability of stable computing even when the difference of shell energies within a supershell is several times higher than the temperature. Its use also yields twofold benefits in computer time compared to the original formula of Ref. [49] (implying that the partition functions should first be normalized): there is no need to solve the equation for the normalization factor, and furthermore, running a single double cycle gives all partition functions for supershell occupation numbers  $1 \leq Q_{\sigma} \leq Q_{\sigma}^{\max}$ , while the original formula of Ref. [49] should be reused for each individual occupation number.

Consider next three different methods to calculate ionization balance. The first method (method I) implies that the first-order correction to the configuration energy  $E_C^{(1)}$  is omitted. In this case, there is no need to partition the total set of electron shells into a number of supershells and then perform the summation over the SCs: the results will remain unchanged if all the shells are gathered into a single supershell. In such a supershell, energy differences of individual shells may, however, far exceed the temperature and therefore it is desirable to calculate the partition function  $\bar{U}_Q^{(0)}(\mathbf{g}) = U_Q^{(0)}(\mathbf{g}) \exp(\beta Q \tilde{\varepsilon}_{\min}^Q)$ , where  $\tilde{\varepsilon}_{\min}^Q = \min\{\tilde{\varepsilon}_s^{(Q)}\}$ , just with the recursion relation of Ref. [49] by going to the normalized partition function, rather than with the simplified Eq. (30). Here, the ionization balance is obtained at a low enough computational cost due to a very limited number of partition functions to be calculated.

In the second method (method II), the first-order correction to the energy of each configuration  $E_C^{(1)}$  is replaced by an appropriate first-order correction to the energy of the basic configuration of the  $Q$ -electron ion to which a given configuration belongs. The results are also independent of the partitioning into supershells, and hence all the shells can be gathered into a single supershell so that the partition function

of the relevant  $Q$ -electron ion can be written as

$$U_Q(\mathbf{g}) = \tilde{U}_Q(\mathbf{g}) \exp\left(-\beta E_{C_0^{(Q)}} + \sum_s q_s^{(Q)} \ln w_s^{(Q)}\right), \quad (31)$$

where  $C_0^{(Q)}$  is the basic configuration of a  $Q$ -electron ion,  $q_s^{(Q)}$  are the basic configuration shell occupation numbers, and

$$\tilde{U}_Q(\mathbf{g}) = \bar{U}_Q^{(0)}(\mathbf{g}) \exp\left(\beta \sum_s q_s^{(Q)} (\tilde{\varepsilon}_s^{(Q)} - \tilde{\varepsilon}_{\min}^Q)\right). \quad (32)$$

Substituting Eq. (31) into Eq. (1) yields

$$\frac{c_Q}{c_{Q-1}} = \frac{\tilde{U}_Q(\mathbf{g})}{\tilde{U}_{Q-1}(\mathbf{g})} \exp\left\{\beta\left(E_{C_0^{(Q-1)}} - E_{C_0^{(Q)}} + \mu_e - \Delta\tilde{\mu}_Q\right) + \ln w_\alpha^{(Q)} + \sum_s q_s^{(Q-1)} \ln \frac{w_s^{(Q)}}{w_s^{(Q-1)}}\right\}, \quad (33)$$

where  $\alpha$  is the outer (partially) filled shell in the basic configuration of a  $Q$ -electron ion.

Consider the difference of basic-configuration energies for the neighboring ionization stages in Eq. (33):

$$\begin{aligned} E_{C_0^{(Q-1)}} - E_{C_0^{(Q)}} &= -\varepsilon_\alpha^{(Q)} - \sum_s q_s^{(Q-1)} (\langle s \rangle^{(Q)} - \langle s \rangle^{(Q-1)}) \\ &\quad - \frac{1}{2} \sum_{st} q_s^{(Q-1)} (q_t^{(Q-1)} - \delta_{st}) (\langle s, t \rangle^{(Q)} - \langle s, t \rangle^{(Q-1)}). \end{aligned} \quad (34)$$

In the CP-SC model, we disregard the distinctions in Eqs. (33) and (34) between the matrix elements  $\langle s \rangle$ ,  $\langle s, t \rangle$  and between the occupation probabilities  $w_s$ , relating to the ions of neighboring ionization stages. This is possible to do since the one-electron wave functions, as a rule, are only slightly different for such ions, and one-electron occupation probabilities for the basic configurations of the most abundant ions are generally close to unity. As a result, the term  $\ln w_\alpha^{(Q)}$  may also be omitted in Eq. (33), which then takes the form

$$\frac{c_Q}{c_{Q-1}} = \frac{\tilde{U}_Q(\mathbf{g})}{\tilde{U}_{Q-1}(\mathbf{g})} \exp[\beta(\mu_e - \Delta\tilde{\mu}_Q - \varepsilon_\alpha^{(Q)})]. \quad (35)$$

The most consistent method III employs the SC-averaged first-order correction  $\langle E_C^{(1)} \rangle_\Xi$ . In this case, the equation for the ratio of fractional ion abundances for neighboring ionization stages still takes the form of Eq. (35), while the expression for the partition function  $\tilde{U}_Q(\mathbf{g})$ , unlike Eq. (32), includes the summation over superconfigurations and the difference of the correction  $\langle E_C^{(1)} \rangle_\Xi$  for running superconfiguration  $\Xi$  and the relevant first-order correction to the energy of the basic

TABLE I. Average numbers of bound electrons for the charge-state distributions shown in Fig. 1.

$T$ (eV)	30	100	300	1000
CP-SC, method I	10.94	6.73	2.20	0.25
CP-SC, method II	17.89	10.42	2.48	0.26
CP-SC, method III	17.76	10.42	2.47	0.26
RESEOS, binomial distribution	17.77	10.47	2.52	0.27
RESEOS, Gibbs distribution	17.72	10.47	2.48	0.26

configuration of the  $Q$ -electron ion:

$$\begin{aligned} \tilde{U}_Q(\mathbf{g}) &= \sum_{\Xi \in Q} \left( \prod_\sigma \bar{U}_{Q_\sigma}^{(0)}(\mathbf{g}) \exp\left\{\beta \sum_{\sigma=1}^{N_\sigma} \left[ D^{(Q)}(\sigma) - A^{(Q)}(\sigma, Q_\sigma) - \sum_{s \in \sigma} \langle q_s \rangle_\sigma \left( \sum_{\sigma'=\sigma+1}^{N_\sigma} B^{(Q)}(\sigma', Q_{\sigma'}, s) - C^{(Q)}(s) \right) \right] + \beta E_{C_0^{(Q)}}^{(1)} \right\} \right), \end{aligned} \quad (36)$$

where

$$D^{(Q)}(\sigma) = \sum_{s \in \sigma} q_s^{(Q)} (\tilde{\varepsilon}_s^{(Q)} - \tilde{\varepsilon}_{\min}^\sigma), \quad (37)$$

and the first-order correction to the basic configuration energy, in accordance with the general Eq. (18), has the form

$$E_{C_0^{(Q)}}^{(1)} = \sum_{st} q_s^{(Q)} \left( \frac{1}{2} (q_t^{(Q)} - \delta_{st}) - (q_t^{(Q,s)} - \delta_{st}) \right) \langle s, t \rangle. \quad (38)$$

Evidently, it is reasonable to calculate the correction (38), as well as the quantities  $A^{(Q)}(\sigma, Q_\sigma)$  (20),  $B^{(Q)}(\sigma, Q_\sigma, s)$  (21),  $C^{(Q)}(s)$  (22),  $D^{(Q)}(\sigma)$  (37),  $\langle q_s \rangle_\sigma$  (23), and  $\bar{U}_{Q_\sigma}^{(0)}(\mathbf{g})$  (30) before doing the summation over superconfigurations in Eq. (36).

Figure 1 provides a comparison of the charge-state distributions in iron plasmas at a density  $\rho = 0.01$  g/cm<sup>3</sup> and various temperatures as calculated with the CP-SC model by using methods I–III and with the RESEOS model utilizing configuration probabilities given by the Gibbs distribution, consistently allowing for the first-order correction  $E_C^{(1)}$  (corresponding to method III in the CP-SC model) [54], and by the binomial distribution disregarding  $E_C^{(1)}$ . The related average numbers of bound electrons  $\langle Q \rangle = \sum_Q c_Q Q$  are presented in Table I. In the case of the binomial distribution (14), these numbers are seen to be only slightly different from the values obtained with the first-order correction  $E_C^{(1)}$  included, even though the binomial distribution overestimates the variance of the charge-state distribution at low temperatures (compared to the characteristic energy of pair interaction between bound electrons) [65]. At low temperatures, the CP-SC calculation in the zero-order approximation strongly underestimates the average numbers of bound electrons due to the use of nonoptimal zero-order energies (16), as discussed above. Indeed, the

zero-order approximation implies that the following replacement is done in Eq. (35):

$$\exp[\beta(E_{C_0^{(Q-1)}} - E_{C_0^{(Q)}})] \approx \exp(-\beta \varepsilon_\alpha^{(Q)}) \rightarrow \exp\left[\beta\left(E_{C_0^{(Q-1)}}^{(0)} - E_{C_0^{(Q)}}^{(0)}\right)\right] = \exp\left(-\beta \varepsilon_\alpha^{(Q)} + \beta \sum_s q_s^{(Q-1)}(\varepsilon_s^{(Q-1)} - \varepsilon_s^{(Q)})\right). \quad (39)$$

Since  $(\varepsilon_s^{(Q-1)} - \varepsilon_s^{(Q)}) < 0$ , the charge-state distribution in the zero-order approximation is seen to be shifted to the lower values of  $Q$ , and the shift gets larger as the temperature goes down. Figure 1 shows that the zero-order approximation (16) gives acceptable results only close to the limit of complete ionization and therefore is generally unsuitable for practical use.

However, even the simplified consideration of the first-order electron-electron interaction correction in the CP-SC model (i.e., calculation by method II) enables one to take into account the major part of the effects due to such correction, and, as is seen from Fig. 1, it yields a charge-state distribution being close to that consistently including the correction  $E_C^{(1)}$  with both the chemical-picture CP-SC and average-atom RESEOS models.

It will be shown in Sec. III (see Figs. 2–5) that average ion charges from the CP-SC calculations done by using methods II and III agree either well or satisfactorily with each other in a wide range of material temperatures and densities (except for relatively low temperatures at which the average number of bound electrons is sufficiently large). At the same time, method II handles only a very moderate number of partition functions and therefore has a very low computational cost. This is achieved by making two steps: first, by the replacement of the first-order corrections to the energies of excited electron configurations by a similar correction to the energy of the basic configuration, and second, by the use of a single set of isolated-ion atomic data (matrix elements  $\langle s \rangle$ ,  $\langle s, t \rangle$ ) for all the electron configurations of a given ion species. As a result, the number of arithmetic operations  $K$  required to evaluate all the partition functions in a given iteration of a self-consistent calculation employing method II can be readily estimated as  $\min(g_s, Q^{\max})N_{\text{tot}}(Q^{\max} - Q^{\min})Q^{\max}$ , where  $N_{\text{tot}}$  is the total number of electron shells, and  $Q^{\min}$  and  $Q^{\max}$  are the minimal and maximal numbers of bound electrons for potentially abundant ion species, respectively. For typical values  $N_{\text{tot}} = 100$ ,  $g_s \lesssim 10$ ,  $Q^{\min} \approx 0$ , and  $Q^{\max} \sim 10$ , we therefore get  $K \sim 10^5$ . This is a moderate number enabling one to perform rapid calculations: for a given pair of  $(\rho, T)$  it takes only a few seconds to run the method-II calculation on a conventional 3 GHz PC, i.e., one or two orders of magnitude smaller than for average-atom models. For these reasons, method II is especially suitable for large-scale calculations. Another advantage of method II over method III is that it offers much easier computer implementation.

At this point, we note that the use of a single set of isolated-ion atomic data for each ion species also appears to be advantageous in the context of method III. According to the algorithm described above, this results in the following number of arithmetic operations performed:  $K \sim (Q_\sigma^{\max} - Q_\sigma^{\min})^{N_\sigma} N_{\text{tot}} N_\sigma$ . This number is generally larger than in the case of method II, but it may be small enough to enable one doing calculations at a

lower computational cost as compared to the average-atom models.

It should also be noted here that some results obtained using method II were published earlier in Ref. [6], but the description of the method itself has not been provided thus far. So, this paper presents a detailed description of the method and its validation.

### III. AVERAGE ION CHARGES FROM CHEMICAL-PICTURE AND AVERAGE-ATOM MODELS

The average ion charge is an unobservable physical quantity and therefore cannot generally be defined unambiguously. The average-atom models are intended for use over a wider range of temperature and density conditions than the chemical-picture ones and hence, unlike the chemical-picture models, the average-atom formalism offers several definitions for the average ion charge [19,31,35–42], each with its advantages and disadvantages in different domains of temperatures and densities. We consider four such definitions.

First, the average ion charge can be defined as the number of electrons in the continuum states (with positive energies) within an atomic cell of radius  $r_0 = [3/(4\pi n_i)]^{1/3}$  (the volume of this cell is equal to the average volume per atom). Since in Liberman's model the atomic cell is electrically neutral, such an average ion charge can also be defined as the difference between the charge of the nucleus  $Z$  and the number of bound-state electrons in the atomic cell:

$$\langle Z \rangle = \langle Z \rangle_1 = Z - \sum_s p_s g_s n(\varepsilon_s^{\text{AA}}), \quad (40)$$

where

$$p_s = \int_0^{r_0} (P_s^2(r) + Q_s^2(r)) dr, \quad (41)$$

with  $P_s(r)/r$  and  $Q_s(r)/r$  being the major and the minor radial components of the relativistic wave function, respectively, given by the solution of average-atom model equations.

At the values of the electron-ion Coulomb coupling parameter

$$\Gamma_{ei} = \frac{1}{3} \left( \frac{r_0}{r_{\text{De}}} \right)^2 \lesssim 1, \quad (42)$$

where

$$r_{\text{De}} = \left( 2\pi \beta \langle Z \rangle n_i \frac{I_{-1/2}(\beta \mu_e^{\text{AA}})}{I_{1/2}(\beta \mu_e^{\text{AA}})} \right)^{-1/2} \quad (43)$$

is the electron Debye radius allowing for the degeneracy [66], the semiclassical approximation works well for the continuum electron states. In this case, average ion charge (40) can be calculated quite accurately by using the nonrelativistic

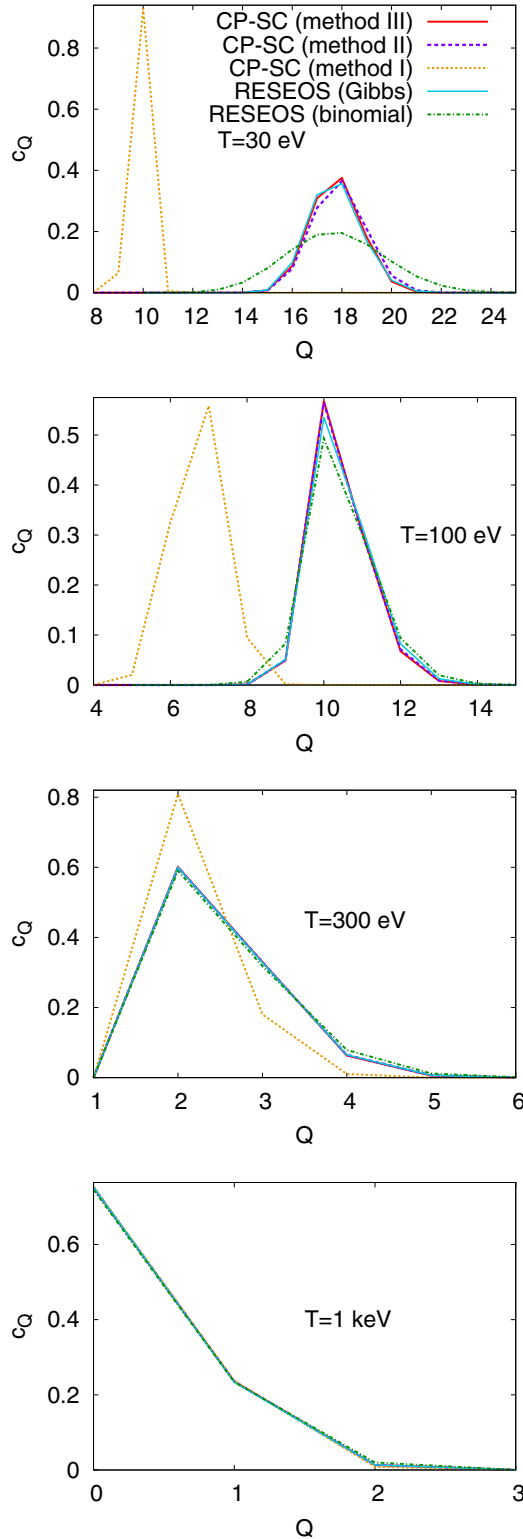


FIG. 1. Relative fractional abundances of  $Q$ -electron ions in iron plasmas at a density  $\rho = 0.01 \text{ g/cm}^3$  and various temperatures as calculated with the CP-SC model by using methods I (orange dashes), II (violet dashes), and III (red solid curves) and with the RESEOS model utilizing configuration probabilities given by the Gibbs (cyan solid curves) and binomial (green dots and dashes) distributions.

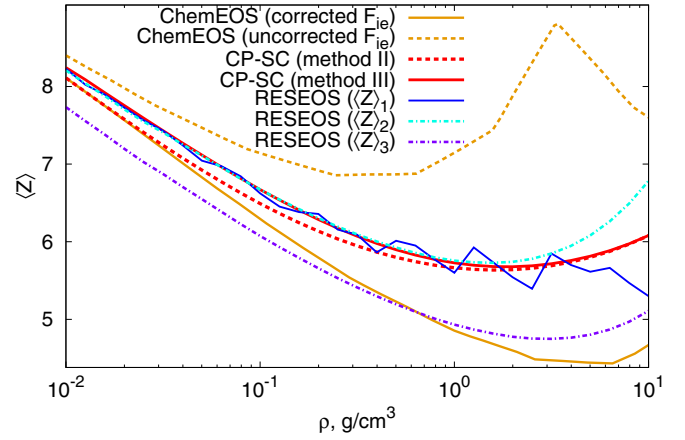


FIG. 2. Average ion charges in an iron plasma at  $T = 30 \text{ eV}$  as calculated with CP-SC (red solid and dashed curves correspond to the use of methods III and II, respectively), RESEOS [blue solid, cyan dashed-dotted, and violet dashed-dotted curves correspond to the use of Eqs. (40), (44), and (45), respectively], and ChemEOS [7,72] (orange solid and dashed curves correspond, respectively, to the calculations with and without correction to the  $F_{ie}$  free-energy term employed).

semiclassical formula

$$\langle Z \rangle_1 \approx \langle Z \rangle_2 = \frac{4\sqrt{2}}{\pi} \int_0^{r_0} r^2 dr \int_0^\infty \sqrt{\varepsilon - V(r)} n(\varepsilon) d\varepsilon, \quad (44)$$

where  $V(r)$  is the electron potential energy. Equation (44) may be considered as an independent wide-range definition of the average ion charge [31,38] and employed at any value of the Coulomb coupling parameter. Though Eq. (44) is derived under the semiclassical approximation, we note that it uses the quantities (chemical potential and the electron potential energy) given by a quantum-mechanical average-atom model rather than by a semiclassical one.

The third frequently used definition of the average ion charge in the average-atom model formally corresponds to the second equality in Eq. (2):

$$\begin{aligned} \langle Z \rangle_3 &= \frac{\sqrt{2}}{\pi^2 \beta^{3/2} n_i} I_{1/2}(\beta \mu_e^{\text{AA}}) \\ &= \frac{4\sqrt{2}}{\pi} \int_0^{r_0} r^2 dr \int_0^\infty \sqrt{\varepsilon} n(\varepsilon) d\varepsilon. \end{aligned} \quad (45)$$

The average ion charge defined in such a way is just the ratio of the free-electron density at  $V(r) = 0$ , i.e., actually at  $r > r_0$ , to the ion density  $n_i$ . Within the atomic cell (at  $r < r_0$ ), the free-electron density usually increases as the radius diminishes due to the growing attraction by the nucleus [the potential energy  $V(r)$  becomes higher in absolute value]. Equation (45) disregards the nonuniformity of the free-electron density and hence systematically underestimates the average ion charge. This underestimation directly follows from the comparison of Eqs. (44) and (45) if it is remembered that  $V(r) < 0$ .

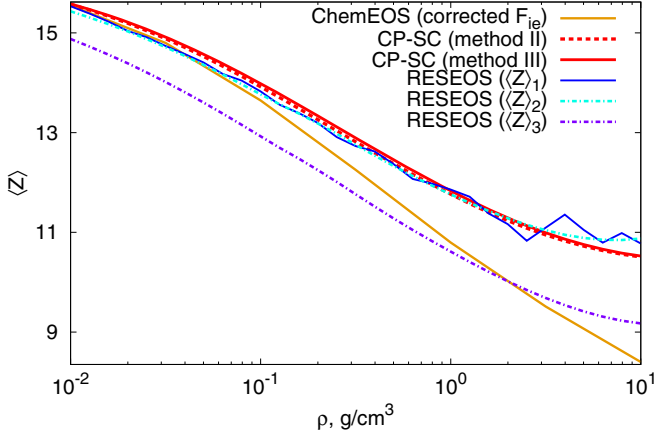


FIG. 3. The same as in Fig. 2 (except for the orange dashed curve) for  $T = 100$  eV.

Finally, the fourth definition of the average ion charge differs from Eq. (45) by the use of the electron density  $n_e(r)$  at the atomic-cell boundary rather than at  $r > r_0$ :

$$\langle Z \rangle_4 = n_e(r_0)/n_i. \quad (46)$$

At  $\Gamma_{ei} \lesssim 1$ , average ion charges from Eqs. (46) and (45) are usually close to each other. However, for strongly coupled plasmas, Eq. (46) in some cases provides better agreement between the calculated and experimental values of various quantities (e.g., electric conductivity in the region of the metal-insulator transition [19]).

Next, we make estimates of the difference  $\delta\langle Z \rangle = \langle Z \rangle_1 - \langle Z \rangle_3 \approx \langle Z \rangle_2 - \langle Z \rangle_3$  assuming that the condition (42) is satisfied and hence the expression under the square root sign in Eq. (44) can be expanded in terms of the small parameter  $V(r)/\varepsilon$ . In this case, the potential energy can be evaluated to an accuracy of  $\sim V(r)/\varepsilon$  in the approximation considering pointlike ion and uniform free-electron density [10]:

$$V(r) \approx -\frac{\langle Z \rangle}{r} \left( 1 - \frac{3r}{2r_0} + \frac{1}{2} \left( \frac{r}{r_0} \right)^3 \right). \quad (47)$$

As a result, we obtain

$$\delta\langle Z \rangle \approx \frac{0.3\langle Z \rangle}{\pi^2 \sqrt{2\beta} n_i r_0} I_{-1/2}(\beta \mu_e^{AA}), \quad (48)$$

$$\frac{\delta\langle Z \rangle}{\langle Z \rangle_3} \approx 0.1 \left( \frac{r_0}{r_{De}} \right)^2 = 0.3\Gamma_{ei}, \quad (49)$$

i.e., Eq. (45) underestimates the average ion charge compared to Eqs. (40) and (44) by a value of the order of  $\Gamma_{ei}$ . Under these conditions (weak Coulomb coupling), the definitions (40) and (44) provide more physically valid results than the definition (45), while in the opposite case of strong Coulomb nonideality, Eq. (40) may severely overestimate average ionization as, according to this equation, all electrons in resonant continuum states [67] are treated as being completely free ones.

In Figs. 2–5, we compare average ion charges calculated for an iron plasma by the CP-SC model [Eq. (2)], Liberman’s model implementation of RESEOS [Eqs. (40), (44), and (45)], and the ChemEOS model [4,7], in which, unlike CP-SC, ion partition functions are found by the detailed account of the

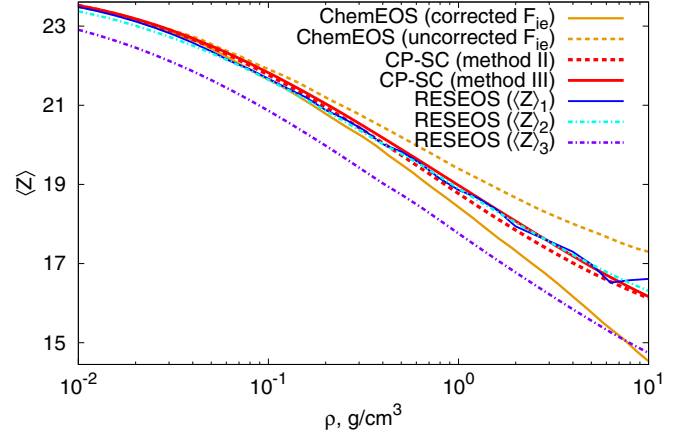


FIG. 4. The same as in Fig. 2 for  $T = 300$  eV.

most probable electronic configurations. The figures show that in the applicability domain of the CP-SC model, the CP-SC values are close to those given by the RESEOS calculations utilizing Eqs. (40) and (44) as the meaning of the definition (40), and hence its semiclassical counterpart (44), is similar to that of the first equality in Eq. (2): average ion charge is just the difference of the nucleus charge and the number of electrons with negative energies.

One can also see that the CP-SC results obtained using two different methods to calculate partition functions—the rather simple method II and the more laborious (but more accurate) method III—are in close agreement. Pronounced differences are found only at the lowest temperature considered— $T = 30$  eV (see Fig. 2). The reason is that the effect due to the consistent treatment of the first-order correction to the configuration energy  $E_C^{(1)}$  grows as the average number of bound electrons increases (with decreasing temperature) because the correction is quadratic in the number of electrons while the configuration energy in the zero-order approximation (16) includes only linear terms. Figure 2 shows that an appropriate inclusion of the first-order electron-electron interaction correction (19) in the context of CP-SC method III improves the

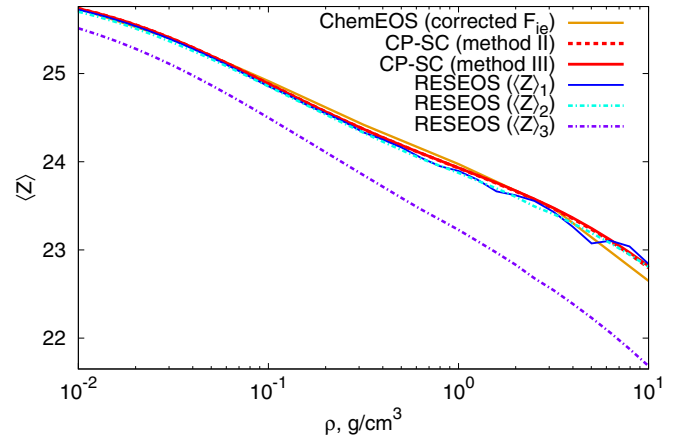


FIG. 5. The same as in Fig. 2 (except for the orange dashed curve) for  $T = 1$  keV. Red solid and dashed curves are seen as almost merged together.

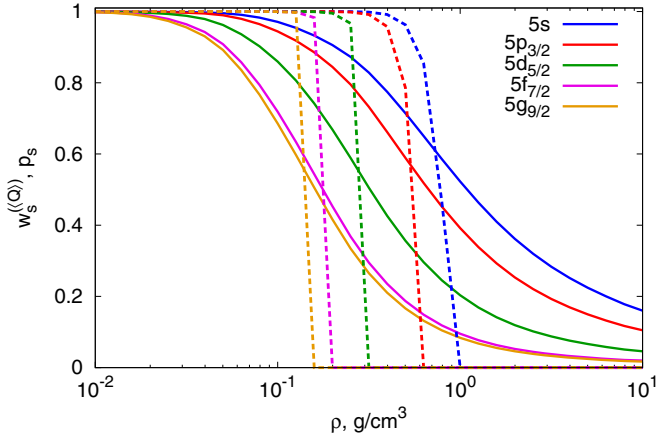


FIG. 6. CP-SC occupation probabilities  $w_s^{(Q)}$  for the  $n = 5$  electron shells in iron plasmas at  $T = 30$  eV (solid curves) and their RESEOS average-atom counterparts (41) (dashed curves of the same colors) vs the plasma material density.

agreement with the RESEOS-calculated data compared to the simplified CP-SC method-II calculation.

An essential distinction of the CP-SC calculations from the RESEOS ones utilizing Eq. (40) stems from the fact that the CP-SC model employs the occupation probabilities of one-electron bound states,  $w_s^{(Q)}(\rho, T)$ , that behave as smoothly varying functions of material density and temperature. In the average-atom model, the quantities  $p_s$  (41)—the integrals of squared relativistic radial wave-function amplitudes over the atomic-cell volume—may be considered as the counterparts of  $w_s^{(Q)}(\rho, T)$ . As the density increases and/or temperature decreases,  $p_s$  first reduces and then vanishes at some density and temperature values ( $\rho_s, T_s$ ) when the relevant shell  $s$  in the average-atom model disappears. The vanishing occurs as an abrupt jump if the orbital quantum number  $l_s \neq 0$  or as a gradual falloff if  $l_s = 0$ . In the chemical-picture model, at densities and temperatures near  $(\rho_s, T_s)$ ,  $w_s^{(Q)}(\rho, T)$  for the most abundant ions also varies from close-to-1 to close-to-0 values, but this variation goes on continuously (without jumps) and far more smoothly than the average-atom  $p_s$  value does. As an illustration, Fig. 6 presents integrals  $p_s$  (41) for the electron shells with principal quantum number  $n = 5$  in iron plasmas at  $T = 30$  eV and various densities calculated by RESEOS and the relevant occupation probabilities  $w_s^{(Q)}$  from the CP-SC model. For a more descriptive comparison with the average-atom model, the probabilities  $w_s^{(Q)}$ , shown in Fig. 6, were obtained for an effective ion with  $\langle Q \rangle = Z - \langle Z \rangle$  bound electrons by interpolating between  $w_s^{(Q)}$  precalculated for ions with nearby integer  $Q$ 's. It is seen that in the CP-SC model, delocalization of bound states under compression proceeds rather slowly: occupation probabilities  $w_s^{(Q)}$  reduce from close-to-1 to close-to-0 values as the density increases by two orders of magnitude. As a result, the CP-SC model gives smooth dependences of the average ion charge on temperature and density. In the average-atom model, bound states are driven to the continuum in rather narrow temperature and density ranges, thus giving rise to irregularities (jumps) in the dependences  $\langle Z \rangle_1(\rho, T)$ . However, in both the average-atom and CP-SC models, bound-electron delocalization takes

place near the same values of  $T$  and  $\rho$  (Fig. 6), and due to this fact the dependences  $\langle Z \rangle_1(\rho, T)$  are essentially close to  $\langle Z \rangle(\rho, T)$  from the CP-SC model, as mentioned above. Although the ways to include the density effects in the CP-SC and average-atom models are formally different, it follows that both models provide a consistent description of these effects.

It should be noted that in the average-atom model, the bound-electron delocalization process is actually not completed when the bound states (with negative energies) disappear as the process generates the relevant density-of-states continuum resonances [67] with the long-lived bound-state properties at further material compression or the temperature lowering. Due to the formation of resonances, all the observable quantities, e.g., thermodynamic functions, chemical potential, and electron density, are free from jumps. Accordingly, there are no jumps in the average ion charges obtained with Eqs. (44), (45), and (46) as those are expressed in terms of the chemical potential, electron density, and potential energy  $V(r)$  directly related to the electron density. In addition, Eq. (44) effectively smooths out the jumps of average ion charge (40). In this context, the values of  $\langle Z \rangle_2$  determined by Eq. (44) behave in a similar way to their CP-SC counterparts. At the same time, the smooth dependence  $\langle Z \rangle_2(\rho, T)$  automatically follows from the equations of Liberman's model [67–71], while getting physically correct smooth dependences  $\langle Z \rangle(\rho, T)$  in the CP-SC model requires additional consideration of the bound-state perturbation due to the plasma ion microfield, thus making the relevant occupation probabilities vary from unity to zero.

ChemEOS results shown in Figs. 2–5 by solid and dashed orange curves differ in approximations for the plasma Helmholtz free energy, which was minimized to derive ionization equilibrium Eqs. (1)–(3). To describe the contribution to the Helmholtz free energy due to the Coulomb interaction of charged particles, the ChemEOS model uses a wide-range analytical approximation of Ref. [73] based on numerical results (solution of the Ornstein-Zernicke equation in the hypernetted-chain approximation, Monte Carlo calculations) and analytical asymptotic expansions. In Ref. [73], this contribution is represented as the sum of three terms:

$$F_C = F_{ii} + F_{ie} + F_{ee}. \quad (50)$$

Here, the term  $F_{ii}$  is responsible for the ion-ion interaction in the one-component plasma approximation [74], i.e., in a system of equally charged pointlike ions moving in a uniform neutralizing background of free electrons,  $F_{ie}$  is a correction to  $F_{ii}$  allowing for the polarization of free-electron gas due to the ion attraction, and  $F_{ee}$  is the exchange-correlation contribution of free electrons.

Dashed orange curves in Figs. 2 and 4 correspond to the original approximation for the Helmholtz free energy of Ref. [73]. In Ref. [7], the term  $F_{ie}$  in Eq. (50) was modified to take account of the finite-ion-size effects (the original approximation was obtained for pointlike ions) enabling one to avoid the nonphysical behavior of average ion charges and thermodynamic functions encountered at high material densities. The average ion charges corresponding to the modified contribution  $F_{ie}$  are shown in Figs. 2–5 by solid orange curves. The CP-SC model also uses the approximation for the Coulomb

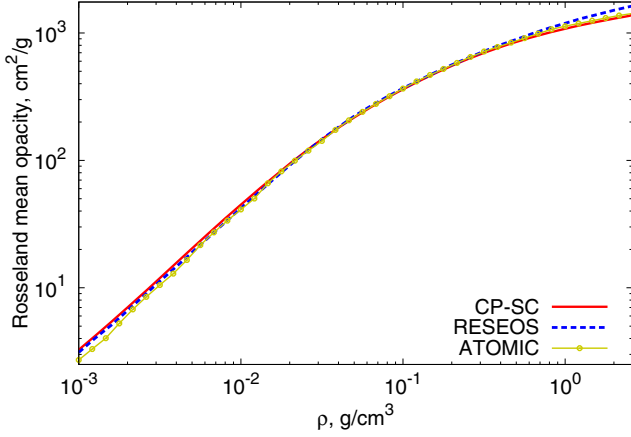


FIG. 7. Rosseland mean opacities of iron plasma at  $T = 250$  eV calculated with CP-SC (red solid curve), RESEOS (blue dashed curve), and ATOMIC [72,75,76] (yellow circles) models.

contribution to the Helmholtz free energy of Ref. [73] with only the leading term  $F_{ii}$  retained. It is seen from Figs. 2–5 that ChemEOS calculations utilizing the original form of  $F_{ie}$  overestimate average ion charges compared to the CP-SC ones and underestimate those when  $F_{ie}$  is modified. This discrepancy gets more pronounced with the increasing role of Coulomb interaction as the density of matter grows and the temperature goes down. Though the CP-SC model disregards the contributions  $F_{ie}$  and  $F_{ee}$ , the results agree well with those obtained by the RESEOS model, which calculates the Coulomb energy considering the nonuniformity of free-electron density and exchange (exchange-correlation) interaction of electrons and therefore allows for the effects described with the  $F_{ie}$  and  $F_{ee}$  terms in the chemical-picture model. This fact provides support for the validity of retaining only the leading ion-ion term  $F_{ii}$  in the wide-range calculations utilizing the analytical approximation for the Coulomb-interaction part of the Helmholtz free energy  $F_C$  [73], and it suggests that further inclusion of the free-electron-gas polarization effect needs to be reconsidered.

Analyzing Figs. 2–5, one should keep in mind that RESEOS, like most of the average-atom models, does not provide correct asymptotics of the Coulomb interaction energy in the limit of weak nonideality (high temperatures and/or low densities of matter). In this limit, the Coulomb interaction is, however, not so important and therefore inaccurate representation of the relevant RESEOS asymptotics has almost no effect on the average ionization (and the total thermodynamic functions), as exemplified by a good agreement with the CP-SC calculations.

So, comparison of the average ion charges shown in Figs. 2–5 suggests that the applicability range of the CP-SC model is wider than that of the current version of the ChemEOS model, at least for mid- $Z$  elements such as iron.

A good overall agreement of average ion charges and corresponding charge-state distributions, which we obtain for average-atom and chemical-picture models, results in the agreement of observable thermodynamic and optical quantities. This is exemplified by Fig. 7, which presents the comparison of Rosseland mean opacities of iron at

$T = 250$  eV calculated by the RESEOS, CP-SC, and ATOMIC [75,76] models (ATOMIC is based on the ChemEOS model). Although the underlying physical models (the Liberman average-atom, chemical-picture CP-SC, and ChemEOS models) and methods employed to calculate opacities (the superconfiguration approach for RESEOS and CP-SC and detailed configuration accounting for ATOMIC) are different, one can see that all the models provide fairly close results.

The second equality in Eq. (2) is formally equivalent to Eq. (45) (keeping in mind the difference of the electron chemical potentials in the chemical-picture and average-atom models), but if the latter equation underestimates the average ion charge, as it disregards the nonuniformity of the free-electron density, Eq. (2) does not provide such an underestimation—see Figs. 2–5. This means that Eq. (2), unlike (45), effectively accounts for the nonuniformity of the free-electron density as the chemical potential  $\mu_e$  in the chemical-picture model is different from its counterpart  $\mu_e^{\text{AA}}$  in the average-atom model ( $\mu_e$  is systematically larger than  $\mu_e^{\text{AA}}$ ). We then evaluate the difference

$$\delta\mu_e = \mu_e - \mu_e^{\text{AA}}, \quad (51)$$

assuming that average ion charges (2) and (40) [or (44)] are identical. So, we have

$$\langle Z \rangle_1 - \langle Z \rangle_3 \approx \frac{\delta\mu_e}{\pi^2 \sqrt{2\beta} n_i} I_{-1/2}(\beta \mu_e^{\text{AA}}) \quad (52)$$

[here we use a commonly known property of the Fermi-Dirac integrals,  $I'_k(x) = k I_{k-1}(x)$  at  $k > 1$ ]. Equating the right-hand sides of Eqs. (52) and (48) yields

$$\delta\mu_e \approx 0.3 \langle Z \rangle / r_0. \quad (53)$$

We note an interesting outcome of Eq. (53) in the context of considering plasma-density effects in the chemical-picture model. Substituting (51) into Eq. (1), one gets

$$\frac{c_Q}{c_{Q-1}} = \frac{U_Q(\mathbf{g})}{U_{Q-1}(\mathbf{g})} \exp \{ \beta [ \mu_e^{\text{AA}} - (\Delta\tilde{\mu}_Q - \delta\mu_e) ] \}. \quad (54)$$

Ionization balance can also be calculated from the average-atom model if one assumes that one-electron wave functions for the most probable ionic configurations are only slightly different from the average-atom ones. In this case, the expression for the ratio of fractional ion abundances for neighboring ionization stages does not include the multiplier  $\exp(-\beta \Delta\tilde{\mu}_Q)$ , while the partition functions are calculated with configuration energies  $\tilde{E}_C^{\text{AA}}$ , which, unlike the configuration energies  $E_C$  of isolated ions, allow for the interaction between bound and free electrons [54,77]. The expression for  $\tilde{E}_C^{\text{AA}}$  can be found in Ref. [54] and, to an accuracy of omitted exchange corrections, may be rewritten in the form

$$\tilde{E}_C^{\text{AA}} = E_C^{\text{AA}} + Q \Delta I. \quad (55)$$

Here,  $\Delta I$  is just the energy of interaction between a bound electron and free ones being responsible for the ionization potential depression (IPD) due to plasma-density effects [78], and  $E_C^{\text{AA}}$  has the same form as the configuration energy of an isolated ion  $E_C$  [Eq. (7)], but  $E_C^{\text{AA}}$  is calculated using one-electron wave functions of the average-atom model. We then assume that in the applicability domain of the CP-SC

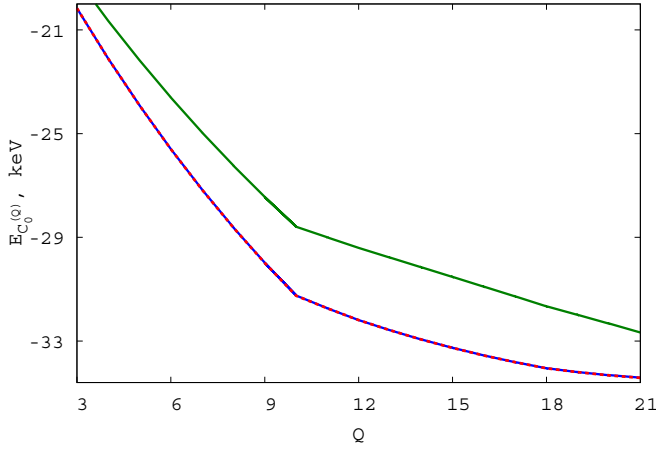


FIG. 8. Basic-configuration average energies of  $Q$ -electron ions of iron. The red dashed curve corresponds to isolated ions ( $E_{C_0^{(Q)}}$ ), the blue solid curve corresponds to the RESEOS calculations at density  $\rho = 10 \text{ g/cm}^3$  and temperatures for which  $\langle Z \rangle \approx Z - Q$  with no account of IPD ( $E_{C_0^{(Q)}}^{\text{AA}}$ ), and the green solid curve corresponds to the similar RESEOS calculations with the account of IPD ( $\tilde{E}_{C_0^{(Q)}}^{\text{AA}}$ ).

model, the average-atom wave functions are close to those of an isolated ion with approximately the same number of bound electrons [this assumption will be examined below (see Fig. 8)], and hence

$$E_C^{\text{AA}} \approx E_C. \quad (56)$$

Then one arrives at the expression

$$\frac{c_Q}{c_{Q-1}} = \frac{U_Q(\mathbf{g})}{U_{Q-1}(\mathbf{g})} \exp[\beta(\mu_e^{\text{AA}} - \Delta I)], \quad (57)$$

where, as in Eq. (54), partition functions are calculated with the configuration energies of isolated ions.

In chemical-picture models, the correction  $\Delta\tilde{\mu}_Q$  to the chemical potential in Eq. (1) is frequently replaced by an estimate of the IPD given by the Stewart-Pyatt model [79],  $\Delta I^{\text{SP}}$  (see, e.g., Ref. [80]). Comparison of Eqs. (54) and (57) suggests that this approach is not sufficiently consistent. In the Stewart-Pyatt model, the IPD is defined as the interaction energy of a bound electron located at the origin of coordinates and external charges (free electrons and external ions) and so it has the same physical meaning as  $\Delta I$  in Eq. (57) and, therefore, as the difference  $\Delta\tilde{\mu}_Q - \delta\mu_e$  in Eq. (54). Because of this, the replacement of  $\Delta\tilde{\mu}_Q$  by  $\Delta I^{\text{SP}}$  leads to an underestimation of the IPD. We illustrate this fact considering an idealized reference system of a uniform ion sphere, i.e., an electrically neutral system of a  $\langle Z \rangle$ -charged central pointlike ion and electrons uniformly distributed inside the sphere of radius  $r_0$  (the system that the system of charges in the average atom is close to as  $\Gamma_{ei} \lesssim 1$  [81–83]). In this case,

$$F_C \approx -0.9\langle Z \rangle^2/r_0, \quad (58)$$

and, if the deviation of occupation probabilities  $w_s$  from unity is neglected, then for the most abundant ions

(with  $Q \approx Z - \langle Z \rangle$ ),

$$\Delta\tilde{\mu}_Q \approx 1.8\langle Z \rangle/r_0, \quad (59)$$

$$\Delta\tilde{\mu}_Q - \delta\mu_e \approx 1.5\langle Z \rangle/r_0. \quad (60)$$

The difference (60) is just the value of IPD given by the Stewart-Pyatt model for the uniform-ion-sphere system, being coincident with  $\Delta I$  in Eq. (55) found for a pointlike ion in the uniform free-electron background, and so the replacement of  $\Delta\tilde{\mu}_Q$  by  $\Delta I^{\text{SP}}$  would lead to the underestimation of the IPD by a factor of 1.25. We note that the correction  $\Delta\mu_e = 1.8\langle Z \rangle/r_0$  was obtained earlier in Ref. [84].

Thus, the chemical-picture and average-atom models consistently describe the IPD due to the plasma-density effects if Eq. (1) in the chemical-picture model includes the variational correction (4) rather than just the value of IPD from the Stewart-Pyatt model or closely related models such as the ion-sphere model [81–83,85–88].

Now, we should check the validity of approximation (56) being essential in the analysis of the relation between IPD in the average-atom and chemical-picture models. The inaccuracy of Eq. (56) grows with increasing material density due to the deviation of electron wave functions found at finite material density from those in isolated ions. Figure 8 presents the comparison of average energies  $E_{C_0^{(Q)}}$ ,  $E_{C_0^{(Q)}}^{\text{AA}}$ , and  $\tilde{E}_{C_0^{(Q)}}^{\text{AA}}$  for basic configurations of various ion species in an iron plasma at the highest density encountered in Figs. 2–5 ( $\rho = 10 \text{ g/cm}^3$ ). For each number of bound electrons  $Q$ , the average-atom (RESEOS) values  $E_{C_0^{(Q)}}^{\text{AA}}$  and  $\tilde{E}_{C_0^{(Q)}}^{\text{AA}}$  were calculated at a temperature for which  $\langle Z \rangle \approx Z - Q$ , and the IPD in Eq. (55) was set equal to its value from the uniform ion sphere model:  $\Delta I = 1.5\langle Z \rangle/r_0$ . One can see that for the cases considered in Figs. 2–5, the relation (56) is indeed valid: the difference between  $E_{C_0^{(Q)}}$  and  $E_{C_0^{(Q)}}^{\text{AA}}$  is less than 0.1%, i.e., much smaller than the difference between  $E_{C_0^{(Q)}}^{\text{AA}}$  and  $\tilde{E}_{C_0^{(Q)}}^{\text{AA}}$ . Hence, in the applicability domain of the CP-SC model (when the pressure ionization is not essential), the difference between electron wave functions in isolated ions and those obtained for finite material density is rather small and does not affect our conclusions on the relation between the CP-SC and RESEOS values of chemical potentials and IPD.

The systematic difference between electron chemical potentials in the chemical-picture and average-atom models is also essential when comparing the relevant thermodynamic functions. This can be illustrated by the following example. Let us assume again that Eq. (53) is valid while Eq. (58) includes the additional exchange-correlation term  $F_{ee}$ :

$$F_C \approx -0.9\langle Z \rangle^2/r_0 + F_{ee}. \quad (61)$$

The average-atom electron pressure evaluated using the semiclassical approximation for free electrons reads (see Ref. [10])

$$P_e^{\text{AA}} \approx \frac{2\sqrt{2}}{3\pi^2 \beta^{5/2}} I_{3/2}(\beta \mu_e^{\text{AA}}) + n_i^2 \frac{\partial F_{ee}}{\partial n_i} \quad (62)$$

(we omitted here the contribution of bound electrons, which is generally small). At the same time, in the chemical-picture model, the electron pressure includes the “ideal” free-electron

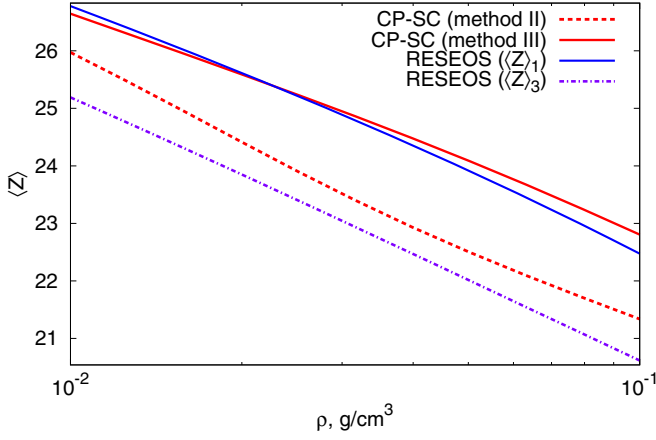


FIG. 9. Average ion charges in a lead plasma at  $T = 100$  eV as calculated with CP-SC (red solid and dashed curves correspond to the use of methods III and II, respectively) and RESEOS [blue solid and violet dashed-dotted curves correspond to the use of Eqs. (40) and (45), respectively].

contribution, which is formally equivalent to the first term in Eq. (62) and the correction due to Coulomb nonideality:

$$\begin{aligned}
 P_e &\approx \frac{2\sqrt{2}}{3\pi^2 \beta^{5/2}} I_{3/2}(\beta \mu_e) + n_i^2 \frac{\partial F_C}{\partial n_i} \approx \frac{2\sqrt{2}}{3\pi^2 \beta^{5/2}} \\
 &\times I_{3/2}[\beta(\mu_e^{AA} + \delta\mu_e)] - \frac{0.3\langle Z \rangle^2}{r_0} n_i + n_i^2 \frac{\partial F_{ee}}{\partial n_i} \approx P_e^{AA} \\
 &+ \beta \delta\mu_e \frac{\sqrt{2}}{\pi^2 \beta^{5/2}} I_{1/2}(\beta \mu_e^{AA}) - \frac{0.3\langle Z \rangle^2}{r_0} n_i \approx P_e^{AA}.
 \end{aligned} \quad (63)$$

So, in this approximation the term with  $\delta\mu_e$  counterbalances the Coulomb nonideality term  $n_i^2 \frac{\partial F_{ii}}{\partial n_i}$ , which is formally missing in the average-atom pressure and, as a result, the average-atom and chemical-picture pressures approximately coincide.

While the distinctions between the CP-SC results obtained with the use of methods II and III remain moderate for iron even at  $T \sim 30$  eV (Fig. 2), similar calculations for heavy elements may show more essential disagreement of the relevant values of  $\langle Z \rangle$  at relatively low temperatures when the average number of bound electrons is sufficiently large. To illustrate this, Fig. 9 presents average ion charges of lead at  $T = 100$  eV calculated with the CP-SC and RESEOS models. Here, the CP-SC calculation by method II underestimates average ion charge by 0.7–1.6 unities compared to the use of method III. Approximately the same underestimation is obtained in the RESEOS calculation done with Eq. (45) compared to that employing Eq. (40), which provides more physically valid results under the conditions considered ( $\Gamma_{ei} < 1$ ). The use of method III instead of method II in the CP-SC model gives better agreement with the RESEOS results obtained with Eq. (40).

It should be noted that the case illustrated by Fig. 9 is rather difficult to calculate by the chemical-picture model due to a large number of electron configurations occurring with substantial probabilities. Detailed accounting of those (like, e.g., in the ChemEOS model) is computationally impractical,

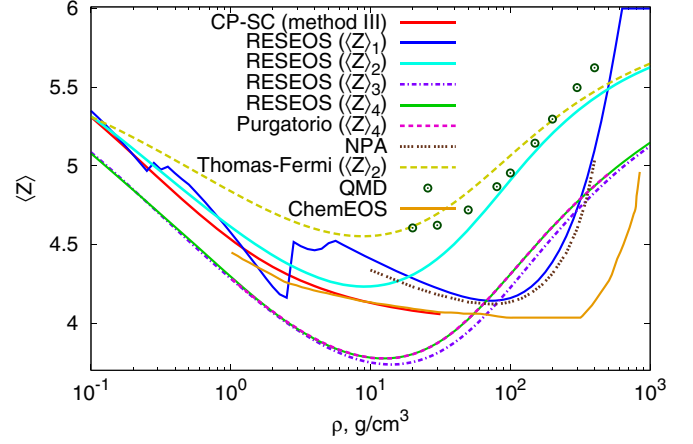


FIG. 10. Average ion charges in a carbon plasma at  $T = 100$  eV as calculated with the CP-SC (using method III—red solid curve), RESEOS [blue, cyan, and green solid curves correspond to the use of Eqs. (40), (44), and (46), respectively, and violet dashed-dotted curve—to the use of Eq. (45)], Thomas-Fermi [using Eq. (44)—yellow dashed curve], Purgatorio [45] [using Eq. (46)—magenta dashed curve], ChemEOS (ATOMIC) [45] (orange solid curve), and NPA [89] (brown dots) models along with the data of Ref. [45] from the QMD dynamic-conductivity calculations utilizing the Kubo-Greenwood formula (dark-green circles).

thus making the use of the superconfiguration approach highly desirable.

To conclude, we consider the dependence of the carbon-plasma average ion charges on the material density at  $T = 100$  eV (Fig. 10). In this case, two methods to calculate the ion partition function in the CP-SC model, i.e., methods II and III, give very close results (as the number of bound electrons in carbon ions is small), and so only the calculations by method III are shown in Fig. 10. Formally, the equations of the CP-SC model can be solved up to very high densities. However, in carbon plasmas at  $T = 100$  eV and  $\rho \gtrsim 10 - 30$  g/cm<sup>3</sup>, of great importance is the effect of pressure ionization providing the growth of average ionization and specific internal energy under compression. The CP-SC model does not reproduce this growth correctly (as it uses the electron wave functions and corresponding matrix elements  $\langle s \rangle$  and  $\langle s, t \rangle$  for isolated ions), and therefore the relevant CP-SC curve in Fig. 10 is truncated at the density  $\rho = 32$  g/cm<sup>3</sup>. As in the case of iron (Figs. 2–5), one can see that the CP-SC average ion charges are generally close to those found with RESEOS in the CP-SC applicability domain by using Eqs. (40) and (44). The dependences  $\langle Z \rangle(\rho)$  obtained both with the CP-SC model and with the semiclassical Eq. (44) effectively smooth out the jumps and irregularities of average ion charge (40) caused by the disappearance of bound-electron states in the average-atom model under the pressure ionization. At low and moderately high ( $\rho \lesssim 10 - 30$  g/cm<sup>3</sup>) densities, Eqs. (45) and (46) underestimate the average ion charge since, as has already been mentioned, these equations do not allow for the nonuniformity of the free-electron density within the atomic cell. In addition to the RESEOS calculations, Fig. 10 also presents the calculations of Ref. [51] performed with the use of Eq. (46) with an alternative Liberman's model

implementation—the Purgatorio code [51]. As one would expect, the RESEOS and Purgatorio calculations following the same definition of the average ion charge provide very close results.

In the high-compression regime ( $\rho \gtrsim 10 - 30 \text{ g/cm}^3$ ), one can observe the large spread in the average ion charges obtained under different approximations. The average ion charge given by Eq. (40) rapidly grows at  $\rho > 100 \text{ g/cm}^3$  as the wave function of the  $1s$  shell is being delocalized outside the atomic cell [under compression, the value of  $p_{1s}$  (41) decreases from unity to zero]. The ChemEOS model qualitatively reproduces this rapid growth but with a shift to higher densities probably due to the approximation employed to evaluate the free-energy term  $F_{ie}$  (50). At the same time, the average ion charge given by the neutral pseudoatom (NPA) model of Dharma-wardana [89] agrees well with the RESEOS one calculated using Eq. (40) (here shown are the results of Ref. [89] obtained by imposing the Friedel sum rule). Unlike the Liberman model implemented in RESEOS, the NPA model consistently accounts for the effect of spatial ion correlations. The agreement of the RESEOS and NPA results suggests that in this case a simple representation of the ion-ion pair correlation function employed in the Liberman model, i.e.,  $g(r) = \theta(r - r_0)$ , where  $\theta(x)$  is the Heaviside function, does not lead to considerable inaccuracies in average ion charge.

Equations (44), (45), and (46) predict a smoother growth with increasing density as compared to Eq. (40) and the calculations done with the ChemEOS and NPA models. Unlike the lower densities, in this case it is difficult to identify the definition of average ion charge yielding more accurate results in the average-atom model since a considerable part of electrons occupy the states with the properties being intermediate between those of bound and purely free-electron states, and hence the average ion charge loses its clear physical interpretation implied in the chemical-picture representation of ionized matter as an interacting mixture of free electrons and ions with various numbers of bound electrons. Thus, the physical meaning of the calculated average ion charge may essentially depend on a specific model, and so the comparison of average ion charges obtained from various models should be made with caution. One can, however, try to relate the average ion charge to one or another observable. For example, in Ref. [45] average ion charge is determined from the sum rule for dynamic conductivity calculated with use of *ab initio* quantum molecular dynamics (QMD) simulations [90] and the Kubo-Greenwood formula [91–93] with the account only of the electron transitions within the conduction band. It is seen from Fig. 10 that Eq. (44) provides the closest agreement with the results obtained in this way. Figure 10 therefore shows that in the context of an average-atom model with a quantum-mechanical description of electrons (such as the Liberman model), Eq. (44) provides reasonable agreement with the QMD calculations when the density of matter is high enough, and good agreement with the chemical-picture results at low densities. This suggests that Eq. (44) can be used in various wide-range models of thermophysical properties of ionized matter employing the results of average-ion-charge calculations as an input data. Here we also note that reasonable agreement with the *ab initio* results of Ref. [45] may be achieved if one evaluates average ion charge with Eq. (44)

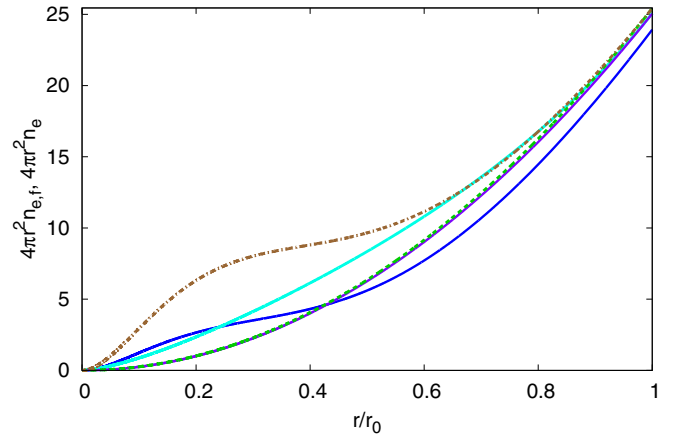


FIG. 11. Radial distributions of free-electron density,  $4\pi r^2 n_{e,f}(r)$ , for carbon at  $T = 100 \text{ eV}$  and  $\rho = 200 \text{ g/cm}^3$  corresponding to average ion charges defined by Eqs. (40) (blue solid curve), (44) (cyan solid curve), (45) (violet solid curve), and (46) (green dashed curve), along with the total radial electron density  $4\pi r^2 n_e(r)$  (brown dashed-dotted curve).

in the context of the semiclassical Thomas-Fermi model [94] (see Fig. 10). In this case, Eq. (44), however, overestimates the average ion charge at low densities as the Thomas-Fermi model disregards quantum shell-structure effects.

It seems likely that the best agreement of the average ion charge (44) with the *ab initio* data of Ref. [45] may be explained in terms of the electron density, which is the key quantity in the density functional theory. Figure 11 presents a comparison of the free-electron density distributions  $n_{e,f}(r)$  corresponding to various definitions of average ion charge, so that  $\langle Z \rangle = 4\pi \int_0^{r_0} r^2 n_{e,f}(r) dr$ . Physically, electrons located near the atomic-cell boundary may be considered as being the free ones since they can move from one cell to another. Equations (45) and (46) underestimate  $n_{e,f}(r)$  near  $r = r_0$  as these average-ion-charge definitions themselves do not allow for the nonuniformity of free-electron density. Equation (40) predicts a considerable contribution of the bound electron density to the total one near  $r = r_0$  because in this case the  $1s$  bound state is not completely localized within the atomic cell (see Fig. 10). As one can see from Fig. 11, under the conditions considered, only the definition of average ion charge (44) ensures that nearly all the electrons at  $r \simeq r_0$  (approximately at  $r/r_0 > 0.6$ ) appear to be the free ones.

#### IV. CONCLUSION

We have analyzed various methods to calculate ion partition functions in the context of the superconfiguration approach implemented in our chemical-picture CP-SC model. It is shown that the calculation of partition functions with the configuration energies found in the zero-order approximation with respect to the electron-electron interaction strongly overestimates average ion charge and is therefore unsuitable for practical use. The realistic description of ionization balance is possible if the first-order corrections to the configuration energies due to the electron-electron interaction are taken into account. We have proposed a simplified method to calculate these corrections enabling one to significantly speed up the

calculations. The method implies that the first-order corrections to the energies of excited electron configurations due to the electron-electron interaction may be replaced by a similar first-order correction to the energy of the basic configuration of an ion with the same number of bound electrons. In most cases (except for heavy elements at  $T \lesssim 100$  eV), this simplification is shown to yield approximately the same results as those obtained with the consistent account of these corrections in the superconfiguration approach.

We have performed the comparisons of average ion charges in iron, lead, and carbon plasmas along with the charge-state distributions (for iron) obtained from the calculations done by the CP-SC model and by the Liberman average-atom model implemented in the RESEOS code. Considering two definitions of average ion charge most frequently employed in Liberman's model—the difference of the nuclear charge and the number of bound-state electrons in the atomic cell (40) and the ratio of the free-electron density outside the atomic cell to the ion density (45)—the first definition was shown to give the results being close to those obtained with the CP-SC model. Although the definition (45) is formally similar to Eq. (2) employed to solve the modified Saha equations of the chemical-picture model, actually it underestimates the average ionization since it does not account for the spatial nonuniformity of the free-electron density. At the same time, Eq. (2), unlike Eq. (45), implicitly accounts for the nonuniformity of the free-electron density, leading to the systematic difference  $\delta\mu_e$  of chemical potentials in the chemical-picture and average-atom models. This difference was estimated analytically in the limit of weak electron-ion nonideality [Eq. (53)]. In addition, we provided estimations indicating that the difference  $\delta\mu_e$  does not lead to the disagreement of IPD and thermodynamic functions obtained from the chemical-picture and average-atom models.

A good agreement between the CP-SC and RESEOS calculations is obtained if the Coulomb interaction of charged particles in the CP-SC model is described under the one-component plasma approximation [74] considering a system of equally charged pointlike ions moving in a uniform neutralizing background of free electrons. Comparison with

the calculations done by using another chemical-picture model ChemEOS [4,7] additionally allowing for the free-electron-gas polarization effect due to the ion attraction both with the original and modified (allowing for the finite-ion-size effects) versions of wide-range analytical approximation of Ref. [73] showed that such methods of considering this effect worsen the agreement with the RESEOS data taking into account the nonuniformity of free-electron density. This fact provides support for the validity of using the one-component plasma approximation [74] to represent the Coulomb interaction in the chemical-picture model and suggests that further inclusion of the free-electron-gas polarization effect needs to be reconsidered.

Considering an iron plasma at  $T = 250$  eV, we have shown that the Rosseland mean opacities obtained from the CP-SC, RESEOS, and ATOMIC models agree fairly well with each other. This additionally indicates that charge-state distributions obtained from these models are close to each other as the opacities are known to be very sensitive to the relative abundances of the ions present.

A good overall agreement of average ion charges, charge-state distributions, and Rosseland mean opacities we obtained using the CP-SC and Liberman models may enhance the reliability of the calculated thermophysical plasma properties. On the one hand, this indicates that well-known troubles with the average-atom model, namely the neglect of the orbital relaxation effect (i.e., the distinction of one-electron wave functions referring to different electron configurations) and incorrect asymptotics of the Coulomb interaction energy in the limit of weak nonideality, do not lead to pronounced inaccuracies. On the other hand, a good agreement of the thermophysical data obtained with the average-atom and CP-SC models for moderately nonideal plasma at  $\Gamma_{ei} \lesssim 1$  suggests that the density effects in the CP-SC model are appropriately taken into account (via the occupation-probability formalism and the Coulomb interaction term in the Helmholtz free energy). We can therefore conclude that even for such values of the Coulomb coupling parameter, the physical accuracy of the CP-SC model is approximately the same as that of the Liberman model (or another similar average-atom model).

- 
- [1] W. Ebeling, W. D. Kraeft, and D. Kremp, *Theory of Bound States and Ionization Equilibrium in Plasmas and Solids* (Akademie-Verlag, Berlin, 1977).
- [2] W. Däppen, L. Anderson, and D. Mihalas, *Astrophys. J.* **319**, 195 (1987).
- [3] D. G. Hummer and D. Mihalas, *Astrophys. J.* **331**, 794 (1988).
- [4] P. Hakel and D. P. Kilcrease, in *Atomic Processes in Plasmas: 14th APS Topical Conference on Atomic Processes in Plasmas 19-22 April 2004, Santa Fe, New Mexico*, AIP Conf. Proc. No. 730 (AIP, Melville, NY, 2004), pp. 190–199.
- [5] A. Y. Potekhin, G. Massacrier, and G. Chabrier, *Phys. Rev. E* **72**, 046402 (2005).
- [6] P. A. Loboda, V. V. Popova, and A. A. Shadrin, *Contrib. Plasma Phys.* **49**, 738 (2009).
- [7] D. P. Kilcrease, J. Colgan, C. J. Fontes, and M. E. Sherrill, *High Energy Density Phys.* **16**, 36 (2015).
- [8] J. Bauche, C. Bauche-Arnoult, and O. Peyrusse, *Atomic Properties in Hot Plasmas, From Levels to Superconfigurations* (Springer International Publishing, Cham, Switzerland, 2015).
- [9] J. Zeng, Y. Li, Y. Hou, and J. Yuan, *Phys. Rev. E* **107**, L033201 (2023).
- [10] A. F. Nikiforov, V. G. Novikov, and V. B. Uvarov, *Quantum-statistical Models of Hot Dense Matter. Methods for Computation Opacity and Equation of State* (Birkhauser, Basel, 2005).
- [11] D. C. Swift, T. Lockard, R. G. Kraus, L. X. Benedict, P. A. Sterne, M. Bethkenhagen, S. Hamel, and B. I. Bennett, *Phys. Rev. E* **99**, 063210 (2019).
- [12] T. Blenski, R. Piron, C. Caizergues, and B. Cichocki, *High Energy Density Phys.* **9**, 687 (2013).
- [13] W. Kohn and L. J. Sham, *Phys. Rev.* **140**, A1133 (1965).
- [14] N. D. Mermin, *Phys. Rev.* **137**, A1441 (1965).

- [15] T. Blenski, A. Grimaldi, and F. Perrot, *J. Quant. Spectrosc. Radiat. Transf.* **65**, 91 (2000).
- [16] J.-C. Pain and T. Blenski, *J. Quant. Spectrosc. Radiat. Transf.* **81**, 355 (2003).
- [17] J.-C. Pain, G. Dejonghe, and T. Blenski, *J. Quant. Spectrosc. Radiat. Transf.* **99**, 451 (2006).
- [18] G. Massacrier, A. Y. Potekhin, and G. Chabrier, *Phys. Rev. E* **84**, 056406 (2011).
- [19] P. A. Sterne, S. B. Hansen, B. G. Wilson, and W. A. Isaacs, *High Energy Density Phys.* **3**, 278 (2007).
- [20] N. Wetta and J.-C. Pain, *Phys. Rev. E* **102**, 053209 (2020).
- [21] C. E. Starrett, *High Energy Density Phys.* **19**, 58 (2016).
- [22] R. Redmer, *Phys. Rev. E* **59**, 1073 (1999).
- [23] S. Kuhlbrodt and R. Redmer, *Phys. Rev. E* **62**, 7191 (2000).
- [24] S. Bastea, *Phys. Rev. E* **71**, 056405 (2005).
- [25] P. Arnault, *High Energy Density Phys.* **9**, 711 (2013).
- [26] S. H. Glenzer and R. Redmer, *Rev. Mod. Phys.* **81**, 1625 (2009).
- [27] A. N. Souza, D. J. Perkins, C. E. Starrett, D. Saumon, and S. B. Hansen, *Phys. Rev. E* **89**, 023108 (2014).
- [28] C. E. Starrett and D. Saumon, *Phys. Rev. E* **92**, 033101 (2015).
- [29] W. Ebeling, A. Förster, V. E. Fortov, V. K. Gryaznov, and A. Polishchuk, *Thermophysical Properties of Hot Dense Plasmas* (Tuebner Verlagsgesellschaft, Stuttgart-Leipzig, 1991).
- [30] C. E. Starrett and D. Saumon, *Phys. Rev. E* **93**, 063206 (2016).
- [31] A. A. Ovechkin, P. A. Loboda, A. L. Falkov, and P. A. Sapozhnikov, *Phys. Rev. E* **103**, 053206 (2021).
- [32] S. H. Glenzer, G. Gregori, R. W. Lee, F. J. Rogers, S. W. Pollaine, and O. L. Landen, *Phys. Rev. Lett.* **90**, 175002 (2003).
- [33] D. Kraus, D. A. Chapman, A. L. Kritcher, R. A. Baggott, B. Bachmann, G. W. Collins, S. H. Glenzer, J. A. Hawreliak, D. H. Kalantar, O. L. Landen, T. Ma, S. LePape, J. Nilsen, D. C. Swift, P. Neumayer, R. W. Falcone, D. O. Gericke, and T. Döppner, *Phys. Rev. E* **94**, 011202(R) (2016).
- [34] M. Z. Mo, Z. Chen, S. Fourmaux, A. Saraf, S. Kerr, K. Otani, R. Masoud, J. C. Kieffer, Y. Tsui, A. Ng, and R. Fedosejevs, *Phys. Rev. E* **95**, 053208 (2017).
- [35] M. S. Murillo, J. Weisheit, S. B. Hansen, and M. W. C. Dharma-wardana, *Phys. Rev. E* **87**, 063113 (2013).
- [36] J. Chihara, *High Energy Density Phys.* **19**, 38 (2016).
- [37] S. Kiyokawa and J. Chihara, *High Energy Density Phys.* **23**, 228 (2017).
- [38] V. M. Elkin, V. N. Mikhaylov, A. A. Ovechkin, and N. A. Smirnov, *J. Phys.: Condens. Matter* **32**, 435403 (2020).
- [39] G. Faussurier and C. Blancard, *Phys. Plasmas* **28**, 042710 (2021).
- [40] N. Wetta and J.-C. Pain, *Contrib. Plasma Phys.* **62**, e202200003 (2022).
- [41] J. Clerouin, A. Blanchet, C. Blancard, G. Faussurier, F. Soubiran, and M. Bethkenhagen, *Phys. Rev. E* **106**, 045204 (2022).
- [42] T. J. Callow, E. Kraisler, and A. Cangi, *Phys. Rev. Res.* **5**, 013049 (2023).
- [43] A. S. Polyukhin, S. A. Dyachkov, and P. R. Levashov, [arXiv:2209.11616v1](https://arxiv.org/abs/2209.11616v1) [physics.plasm-ph].
- [44] S. Kiyokawa, *High Energy Density Phys.* **13**, 40 (2014).
- [45] M. Bethkenhagen, B. B. L. Witte, M. Schörner, G. Röpke, T. Döppner, D. Kraus, S. H. Glenzer, P. A. Sterne, and R. Redmer, *Phys. Rev. Res.* **2**, 023260 (2020).
- [46] G. Faussurier, C. Blancard, and M. Bethkenhagen, *Phys. Rev. E* **104**, 025209 (2021).
- [47] D. A. Liberman, *Phys. Rev. B* **20**, 4981 (1979).
- [48] A. Bar-Shalom, J. Oreg, W. H. Goldstein, D. Shvarts, and A. Zigler, *Phys. Rev. A* **40**, 3183 (1989).
- [49] F. Gilleron and J.-C. Pain, *Phys. Rev. E* **69**, 056117 (2004).
- [50] D. A. Liberman, *J. Quant. Spectrosc. Radiat. Transf.* **27**, 335 (1982).
- [51] B. Wilson, V. Sonnad, P. Sterne, and W. Isaacs, *J. Quant. Spectrosc. Radiat. Transf.* **99**, 658 (2006).
- [52] A. Bar-Shalom, J. Oreg, and M. Klapisch, *J. Quant. Spectrosc. Radiat. Transf.* **99**, 35 (2006).
- [53] M. Pénicaud, *J. Phys.: Condens. Matter* **21**, 095409 (2009).
- [54] A. A. Ovechkin, P. A. Loboda, V. G. Novikov, A. S. Grushin, and A. D. Solomyannaya, *High Energy Density Phys.* **13**, 20 (2014).
- [55] A. A. Ovechkin, P. A. Loboda, and A. L. Falkov, *High Energy Density Phys.* **20**, 38 (2016).
- [56] Hartree atomic units  $\hbar = m_e = e = 1$  are used throughout the paper.
- [57] R. D. Cowan, *The Theory of Atomic Structure and Spectra* (University of California Press, Berkeley, CA, 1981).
- [58] R. Karazija, *The Theory of X-ray and Electronic Spectra of Free Atoms. An Introduction* (Mokslas, Vilnius, 1987) (in Russian).
- [59] V. G. Novikov, *High Temp.* **30**, 573 (1992).
- [60] T. Blenski, A. Grimaldi, and F. Perrot, *Phys. Rev. E* **55**, R4889 (1997).
- [61] M. F. Gu, *Can. J. Phys.* **86**, 675 (2008).
- [62] J. Oreg, A. Bar-Shalom, and M. Klapisch, *Phys. Rev. E* **55**, 5874 (1997).
- [63] G. Faussurier, B. G. Wilson, and M. H. Chen, *Phys. Rev. E* **65**, 016403 (2001).
- [64] J.-C. Pain, F. Gilleron, and G. Faussurier, *Phys. Rev. E* **80**, 026703 (2009).
- [65] G. Faussurier, C. Blancard, and A. Decoster, *Phys. Rev. E* **56**, 3474 (1997).
- [66] Expression (42) is the ratio between characteristic values of free-electron-ion Coulomb interaction energy,  $\sim \langle Z \rangle / r_0$ , and electron kinetic energy. For weak degeneracy [ $e^{\beta \mu_e^{\text{AA}}} \ll 1$ , or  $T \gg E_F$ , where  $E_F = \frac{1}{2} (3\pi^2 \langle Z \rangle n_i)^{2/3}$  is the Fermi energy], one has  $\Gamma_{ei} \simeq \langle Z \rangle / (r_0 T)$ , otherwise for strong degeneracy ( $T \ll E_F$ ),  $\Gamma_{ei} \approx 3 \langle Z \rangle / (2r_0 E_F)$ .
- [67] R. M. More, *Adv. At. Mol. Phys.* **21**, 305 (1985).
- [68] W. Kohn and C. Majumdar, *Phys. Rev.* **138**, A1617 (1965).
- [69] A. G. Petschek, *Phys. Lett. A* **34**, 411 (1971).
- [70] A. G. Petschek and H. D. Cohen, *Phys. Rev. A* **5**, 383 (1972).
- [71] V. G. Novikov and A. A. Ovechkin, Keldysh Institute of Applied Mathematics, preprint No. 31 (2009), <https://library.keldysh.ru/preprint.asp?id=2009-31>.
- [72] <http://aphysics2.lanl.gov/opacity/lanl>.
- [73] G. Chabrier and A. Y. Potekhin, *Phys. Rev. E* **58**, 4941 (1998).
- [74] J. P. Hansen, *Phys. Rev. A* **8**, 3096 (1973).
- [75] P. Hakel, M. E. Sherrill, S. Mazevet, J. Abdallah Jr., J. Colgan, D. P. Kilcrease, N. H. Magee, C. J. Fontes, and H. L. Zhang, *J. Quant. Spectrosc. Radiat. Transf.* **99**, 265 (2006).
- [76] J. Colgan, D. P. Kilcrease, N. H. Magee, J. Abdallah Jr., M. E. Sherrill, C. J. Fontes, P. Hakel, and H. Zhang, *High Energy Density Phys.* **14**, 33 (2015).
- [77] R. Piron and T. Blenski, *High Energy Density Phys.* **9**, 702 (2013).
- [78] For simplicity, the values of  $\Delta I$  are assumed to be the same for all the electron shells. This assumption is justified if the

- localization region of bound-electron wave functions is small compared to the atomic-cell volume that is generally valid in the applicability domain of the CP-SC model.
- [79] J. C. Stewart and K. D. Pyatt, *Astrophys. J.* **144**, 1203 (1966).
- [80] F. Jin, J. Zeng, T. Huang, Y. Ding, Z. Zheng, and J. Yuan, *Astrophys. J.* **693**, 597 (2009).
- [81] X. Li and F. B. Rosmej, *Europhys. Lett.* **99**, 33001 (2012).
- [82] X. Li, F. B. Rosmej, V. S. Lisitsa, and V. A. Astapenko, *Phys. Plasmas* **26**, 033301 (2019).
- [83] X. Li and F. B. Rosmej, *Phys. Lett. A* **384**, 126478 (2020).
- [84] G. B. Zimmerman and R. M. More, *J. Quant. Spectrosc. Radiat. Transf.* **23**, 517 (1980).
- [85] G. Massacrier and J. Dubau, *J. Phys. B* **23**, 2459S (1990).
- [86] M. Poirier, *High Energy Density Phys.* **15**, 12 (2015).
- [87] C. A. Iglesias, *High Energy Density Phys.* **30**, 41 (2019).
- [88] J.-C. Pain, *High Energy Density Phys.* **31**, 99 (2019).
- [89] M. W. C. Dharma-wardana, *Phys. Rev. E* **104**, 015201 (2021).
- [90] D. Marx and J. Hutter, *Ab Initio Molecular Dynamics: Basic Theory and Advanced Methods* (Cambridge University Press, Cambridge, 2009).
- [91] R. Kubo, *J. Phys. Soc. Jpn.* **12**, 570 (1957).
- [92] D. A. Greenwood, *Proc. Phys. Soc. London* **71**, 585 (1958).
- [93] G. V. Chester and A. Thellung, *Proc. Phys. Soc. London* **77**, 1005 (1961).
- [94] R. Feynman, N. Metropolis, and E. Teller, *Phys. Rev.* **75**, 1561 (1949).